Separation and Purification Technology 321 (2023) 124195

Contents lists available at ScienceDirect

Separation and Purification Technology

journal homepage: www.elsevier.com/locate/seppur

In-situ immobilization of MIL-100(Fe) on the microchannels in wood aerogel: Efficient persulfate activation toward antibiotic removal

Haihao Peng [a,b], Jing Tong [a,b], Jing Huang [c,*], Zhaohui Yang [a,b,*], Weiping Xiong [a,b], Yuxuan Yao [a,b], Yinping Xiang [a,b], Zhengyong Xu [d]

[a] College of Environmental Science and Engineering, Hunan University, Changsha 410082, PR China
[b] Key Laboratory of Environmental Biology and Pollution Control (Hunan University), Ministry of Education, Changsha 410082, PR China
[c] Institute of Biological and Environmental Engineering, Hunan Academy of Forestry, Changsha 410004, PR China
[d] Hunan Modern Environmental Technology Co. Ltd, Changsha 410004, PR China

ARTICLE INFO

Keywords:
Wood aerogel
MIL-100(Fe)
Persulfate
AOPs
Antibiotic

ABSTRACT

Metal-organic frameworks (MOFs) are potential catalysts for persulfate exciting in antibiotic wastewater treatment while are limited in large-scale application given their powder state. Herein, benefiting from the compatibility and functionalization of natural wood supports, MIL-100(Fe) decorated wood aerogel composites (MIL-100(Fe)/WA) were constructed by chemical treatment and in-situ solvothermal synthesis. Na_2SO_3/NaOH-H_2O_2 chemical treatment could effectively achieve the partial removal of lignification and hemicellulose in wood, resulting in improved porous characteristics. The corresponding porosity and surface area of WA increased by more than 40% compared with the original wood. Accordingly, after immobilizing MIL-100(Fe) on the microchannels in WA, MIL-100(Fe)/WA-PDS system could efficiently degrade tetracycline (TC), with a satisfied mineralization rate of 64.01% owing to the open porous structure of WA with high accessibility, and its kinetic constant (0.0520 $L{\cdot}mg^{-1}{\cdot}min^{-1}$) was 6.19 times that of MIL-100(Fe)/wood (0.0084). Quenching results and EPR analysis made clear that TC degradation mainly contributed to the produced $O_2^{\cdot-}$, $^1O_2$ and surface-bound radicals ($SO_4^{\cdot-}$, $^{\cdot}OH$). LC-MS further uncovered the possible degradative pathways for TC. Moreover, it was found that MIL-100(Fe)/WA could behave well at pH of 2–10 and towards multiple antibiotics. This work may provide a facial way to apply MOFs-based/wood composites in water treatment.

1. Introduction

The widespread use of antibiotics has already aroused growing attention due to the ecological hazards and health risks they pose. Residual antibiotic in environmental mediums, such as surface water and soil, can induce the accelerating generation of drug-resistant strains with antibiotic resistance genes (ARGs) [1]. The spread of AGRs relying on various vectors will pose more serious environmental issues than antibiotics alone. Consequently, there is a pressing need to eliminate antibiotics from environments employing effective techniques. Currently, numerous means are popular in antibiotic pollution management, such as physical adsorption, extraction technology, bio-treatment, and chemical oxidation [2,3]. Among various heterogeneous catalysis in chemical oxidation, advanced oxidation process (AOP) based on persulfate activation to produce highly active reactive oxygen species (ROS) ($SO_4^{\cdot-}$, $^{\cdot}OH$, $O_2^{\cdot-}$, etc.) for pollution degradation is receiving increased interest, given its convent operation, controllable cost, and satisfying removal efficiency [4,5].

Considering the activation approaches of persulfate by energy transfer (thermal /ultrasonic activation) or electron transfer (alkali/electrochemical/carbon catalyst activation), transition metal activation with low energy consumption and high efficiency is widely studied [6]. Especially, emerging porous metal–organic frameworks (MOFs) comprising organic ligands and metal centers that can act as catalytic active sites for persulfate exciting, are deemed to be potential catalysts that have broad applications ascribed to their superiority in structure and function [7]. Undoubtedly, Fe-MIL in possession of great stability shown in thermal and chemical aspects, low toxicity as well as active Fe (II)/Fe(III) components are desirable. However, the challenges facing Fe-MIL are derived from their powder state with poor processability and applied performance with inevitable loss, vastly limiting their large-scale applications. The strategy of anchoring Fe-MIL into porous

* Corresponding authors at: College of Environmental Science and Engineering, Hunan University, Changsha 410082, PR China (Z. Yang).
E-mail addresses: gavinhj@163.com (J. Huang), yzh@hnu.edu.cn (Z. Yang).

https://doi.org/10.1016/j.seppur.2023.124195
Received 8 February 2023; Received in revised form 10 May 2023; Accepted 24 May 2023
Available online 29 May 2023

supports has proven to be effective, as it keeps accessibility and allows Fe-MIL to be fully utilized. In this way, a great number of macroscopical MOFs-based composites are emerging involving polymer film, carbon cloth, metal mesh, aerogels, etc. Recently, MOFs functioned wood materials integrating both advantages spring up.

Wood belongs to low-cost renewable sources that consist of open cellular structures that intertwined with cellulose, hemicellulose and lignin [8]. The distinct internal vertical channels in wood with ordered pore size and abundant oxygen-containing groups, make wood attractive for MOFs immobilization which can be applied in various fields, as examples of ZIF-8 functionalized-wood solar evaporator achieving the augmenting solar evaporation efficiency [9] and flow-through AgPd/UiO-66@wood catalytic microreactors for continuous controllable hydrogen generation [10]. More research has focused on the application on environmental remediation with MOFs/wood composites. For instance, Guo et al. developed wood membrane decorated with UiO-66 by solvothermal strategy [11]. The unique vertical porous structure combined with mesoporous UiO-66 enhanced fast mass transfer and contact probability, leading to high-efficiency removal of organic contaminants. Subsequent research found that wood anchored with ZIF-8 or NH_2-MIL-53 could effectively eliminate heavy metals via adsorption [12,13]. Nevertheless, a limiting situation is that the comparatively low porosity of natural wood stemmed from their compact cellular structure, somewhat restraining their enhanced performance.

Aiming at the improved structural property, select removal of hemicellulose and lignin in wood through chemical treatment (e.g., $NaClO_2$, Na_2SO_3/NaOH-H_2O_2) to fabricate cellulose-based wood aerogel (WA) with strengthened performance is of increased interest [14,15]. After removing hemicellulose and lignin from wood, the obtained WA can be superior to the original wood, such as excellent mechanical properties, lower density, and higher porosity [16], as an example of hydrophobic wood aerogel delignified using $NaClO_2$ for reusable oil/water separation with flux and high separation efficiency (99.5%) [17]. Thus, WA can be regarded as a more applicable support for loading MOFs compared with the origin wood. Chen et al. immobilized ZIF-67 on the channels in WA to obtain compressible composite adsorbents (ZIF-67@WA), reaching the goal of effective adsorption of antibiotics from water [18]. Another similar research concentrated on the selective extraction of uranium from seawater [19]. Meanwhile, compared with other supports in immobilizing MOFs, such as graphene aerogel [20] or silica nanofibrous membrane [21], which required higher cost or complex preparation process, WA with easy availability, lower cost, and ordered porous structure could be a desired support. Thus, considering the limited studies on MOFs/WA, it is worth to discover their potential in persulfate exciting towards antibiotic removal.

In this work, low-density balsa wood ($\rho = 0.120$ g cm^{-3}) was applied as a wood precursor. WA was prepared through the chemical removal of lignin and hemicellulose of wood employing Na_2SO_3/NaOH and H_2O_2 at high-temperature conditions, as well as freeze drying. Via the solvothermal method, MIL-100(Fe) further in-situ grew on the microchannels of WA to obtain MIL-100(Fe)/WA composites that were used for PDS activation towards tetracycline (TC) degradation. The enhancement of catalytic performance in MIL-100(Fe)/WA-PDS was observed in contrast to MIL-100(Fe)/wood-PDS system. Combined with various characterizations, the performance of catalysts was analyzed. The representative variables that could affect TC degradation such as pH, temperature and co-existing anions were investigated systemically. According to the quenching experiments and EPR, the main reactive oxygen species (ROS) that participated in TC oxidization were identified. The possible catalytic mechanism was proposed, along with its degradation pathways relying on liquid chromatography-mass spectrometry (LC-MS). Moreover, multiple antibiotics and real water for simulating TC removal were conducted. This work provided a facial approach to fabricate MOFs-based WA composites and exploit their potential for persulfate activation towards remediation of antibiotic wastewater.

2. Experiment

2.1. Chemicals

Chemicals applied without being purified further are presented: balsa wood ($\rho = 120$ kg m^{-3}), tetracycline (TC, 99%), ferric trichloride hexahydrate ($FeCl_3{\cdot}6H_2O$, 99%), N, N-dimethylformamide (DMF, 99%), trimesic acid (H_3BTC, 98%), sodium persulfate (PDS, $Na_2S_2O_8$, 98%), sodium bicarbonate ($NaHCO_3$, 99%), sodium sulfate (Na_2SO_4, 99%), sodium chloride (NaCl, 99.5%), trisodium phosphate dodecahydrate ($Na_3PO_4{\cdot}12H_2O$, 98%), sodium carbonate (Na_2CO_3, 99.8%), methanol (MeOH, 99%), tertiary butanol (TBA, 98%), p-benzoquinone (BQ, 98%), sodium azide (NaN_3, 98%) and ultrapure water (18.25 MΩ cm^{-1}).

2.2. Sample fabrication

Wood aerogel (WA): Balsa wood blocks (20 × 10 × 5 mm) were washed using methanol and ultrapure water for removing the impurity. The dried balsa wood blocks were immersed in NaOH (2 M)/Na_2SO_3 (0.5 M) solution at 100 °C for 4 h to eliminate lignin and hemicellulose, and washed using ultrapure water. The washed wood sample was further treated with H_2O_2 solution (2.5 M) for 2 h. The WA was obtained by washing and freeze drying.

MIL-100(Fe)/WA: WA was first added into ferric chloride DMF solution (1.5 mM) in vacuum conditions lasting for 2 h to achieve the full impregnation of Fe ions into WA. Then, 1.9 mmol H_3BTC was dissolved into the mixture which was transferred to a Teflonlined container and reacted for 24 h at 150 °C. MIL-100(Fe)/WA could be obtained by washing with DMF and ultrapure water and following freeze drying.

2.3. Characterizations

The morphological features and corresponding chemical constitution were detected using scanning electron microscopy (SEM, Zeiss Sigma 3000), X-ray diffractometer (XRD, Bruker D8 Advance) and X-ray photoelectron spectrums (XPS, Thermo Scientific K-Alpha). The surface functional groups of samples were analyzed with Fourier transform infrared spectroscopy (FTIR, Thermo Scientific Nicolet iS20). Brunauer-Emmett-Teller (BET) analyzer (Micromeritics ASAP 2460) was employed for N_2 adsorption–desorption test to obtain pore structure characteristics.

2.4. Degradation experiment

In TC degradation, 50 mL TC solution (30 mg L^{-1}) containing PDS (15 mg) was reacted with MIL-100(Fe)/WA (20 × 10 × 5 mm) in conical flasks, shaken at fixed temperatures and 160 rpm. The TC concentration at different intervals was detected via UV–Vis spectra at 357 nm. More information concerning influence variables, quenching experiments, regeneration, etc. was shown in the supporting information.

3. Result and discussion

3.1. Characterizations

Via SEM, morphology change in different samples was obtained. Wood was composed of ordered parallel cavities with open channels. As presented in Fig. 1a, open vertical channels with a diameter of 40–60 μm in wood were observed. Further, it was found that the selective removal of lignin and hemicellulose had no obvious effect on the channels of WA (Fig. 1c-d), as well as the following growing of MIL-100(Fe) on WA (Fig. 1e-f). Thus, the retaining porous structure of WA was conducive to the transfer and contact with the contaminant. Moreover, MIL-100(Fe) grew uniformly on the surface of channels in MIL-100(Fe)/WA (Fig. 1g), demonstrating the effective growth of MIL-100(Fe) on the channels in WA. At the same time, the loaded MIL-100(Fe) on MIL-100

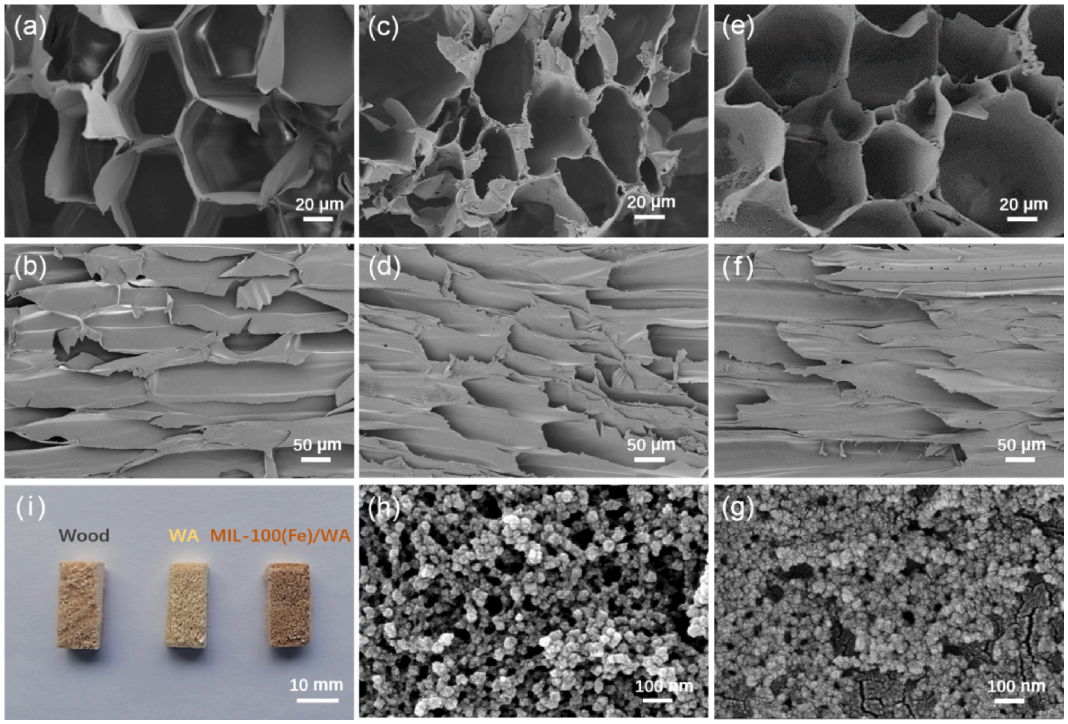

Fig. 1. SEM of wood (a-b), WA (c-d), MIL-100(Fe)/WA (e-g) and MIL-100(Fe) (h); photograph of wood, WA, MIL-100(Fe)/WA (i).

(Fe)/WA was almost the same as MIL-100(Fe) particles in morphology and particle size (Fig. 1h). Thus, the porous channels of WA supplied the desired condition for MOF synthesis with no limitation in MOF growing. The photograph of wood, WA and MIL-100(Fe)/WA in Fig. 1i reflected the change of color in the processing of wood and the maintenance of its structure.

Furthermore, as shown in Fig. 2a, XRD analysis identified the structure of different samples. There were two broad peaks located at 16° and 22° in wood, WA and MIL-100(Fe)/WA, which corresponded to cellulose in these samples [9]. Compared with original wood, the intensity of the two peaks increased in WA. It indicated that NaOH/Na_2SO_3 combing with H_2O_2 system enabled to effectively remove hemicellulose and lignin, thus increasing the crystallinity of cellulose in WA. Meanwhile, the constituent of wood and WA in Fig. 2b also indicated the reduced proportion of lignin and hemicellulose, as well as distinctly increased content of cellulose. With the growing of MIL-100 (Fe) on WA, given the low loading of MIL-100(Fe), only a small peak at 11° belonging to MIL-100(Fe) appeared in MIL-100(Fe)/WA, suggesting the effective immobilization of MIL-100(Fe) on WA.

In Fig. 2c, FTIR distinguished the differences in functional groups for these samples. Clearly, the peaks at 1730 $cm^{-1}$and 1240 cm^{-1} which were recognized as C=O and C-O bonds disappeared in WA. This result reflected the elimination of hemicellulose and lignin in the wood after the treatment of NaOH/Na_2SO_3 and H_2O_2 [22]. Regarding MIL-100(Fe),

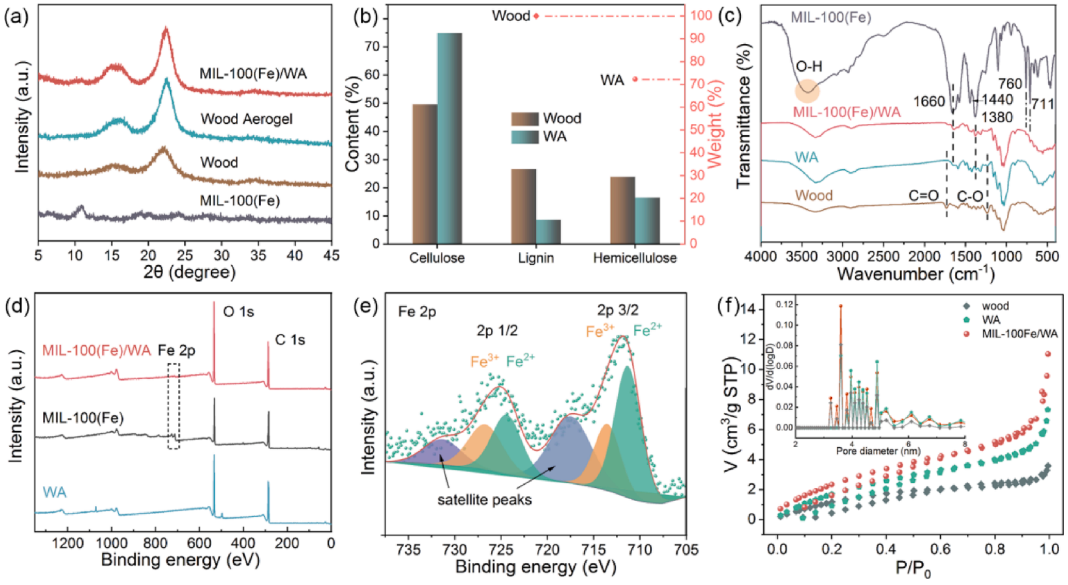

Fig. 2. XRD of different samples (a); the constituents and weight change of wood and WA (b); FTIR (c) and XPS survey (d) of different samples; Fe 2p of MIL-100(Fe)/WA (e); N_2 adsorption–desorption isotherms (f).

at 3400 cm^{-1}, this broad band was assigned as the stretching vibrations of O–H ascribed to free carboxyl groups and adsorbed H_2O [23]. The peaks at 760, 711 and 461 cm^{-1} matched with the bending vibrations of C–H in benzene. The band located in 1660 cm^{-1} belonged to the stretching vibration of carboxylate groups, meanwhile the peaks at 1440 cm^{-1} and 1380 cm^{-1} originated from the asymmetrical and symmetrical vibrational of the -O-C-O- groups [24]. After MIL-100(Fe) growing in WA, those characteristics of MIL-100(Fe) arose in the composites, which indicated the effective combination of MOF and WA. This analysis also accorded with the result from SEM and XRD.

Combined with FTIR, XPS provided clearer evidence about the element composition and valence in different samples. As presented in Fig. 2d, XPS survey clearly provided the exist of C, Fe and O in MIL-100 (Fe), while the peaks of Fe 2p in MIL-100(Fe)/WA were small on account of the low content of Fe (0.5%) according to Table S2, which also suggested the low loading of MIL-100(Fe) on WA. For C 1 s (to Fig. S1a), the curves could be fitted with C–C (284.7 eV), O–C–O/C–O (286.4 eV) and O–C=O (288.1 eV), respectively [25,26]. It was clear that the proportion of C–O–C/C–O in MIL-100(Fe)/WA increased significantly in contrast to that in WA, which was caused by the introduction of C-O in MIL-100 (Fe). The result confirmed the combination of MIL-100(Fe) and WA as well. Regarding MIL-100(Fe)/WA, Fe 2p appeared in Fig. 2e containing Fe 2p 1/2 and Fe 2p 2/3 orbits, at which they were matched with Fe(II) (711.3 eV and 724.4 eV) and Fe(III) (713.5 eV and 726.7 eV) coupled with their satellite peaks [23]. Thus, the existence of Fe in MIL-100(Fe)/WA indicated the successful growing of MIL-100(Fe), and the coexistence of Fe(II) and Fe(III) was conducive to activating persulfate for efficient pollutant removal.

Moreover, the structural changes of porosity, BET surface area and pore distribution during the wood processing and MIL-100(Fe) growing were evaluated. As depicted in Fig. 2f, the N_2 adsorption–desorption curves of wood, WA, and MIL-100Fe belonged to type IV isotherms without obvious hysteresis loops, indicating that mesopores were dominated in these samples [27]. While the type of MIL-100(Fe) was regarded as type I isotherm, identified by microporous adsorption at low pressure with plenty of micropores in the ordered skeleton of MIL-100 (Fe) (Fig. S1b). Considering the low loading of MIL-100(Fe), the isotherm corresponding to MIL-100(Fe)/WA did not change. It was found that after being treated with NaOH/Na_2SO_3 and H_2O_2, the absorbed N_2 rose significantly. This phenomenon suggested the increased porosity when lignin and hemicellulose were removed, creating more pores in wood channels. Simultaneously, the enhanced porosity (0.0113 $cm^3\ g^{-1}$) and BET surface area (8.77 $m^2\ g^{-1}$) compared with WA (0.0055 $cm^3\ g^{-1}$, 6.19 $m^2\ g^{-1}$) also supported this conclusion (Table 1), as well as the enlarged pore sizes, manifesting the effectiveness of this strategy. Further, the growing of MIL-100(Fe) on WA also improved the adsorbed volume, which was stemmed from the high adsorption ability of MIL-100(Fe) through micropores. The corresponding porosity and surface area reached to 0.0169 $cm^3\ g^{-1}$ and 10.38 $m^2\ g^{-1}$, which was caused by the high porosity (0.4062 $cm^3\ g^{-1}$) and huge surface area (764.8 $m^2\ g^{-1}$) of MIL-100(Fe). Nevertheless, MIL-100(Fe) anchoring on the channels in WA led to a decreased pore size (5.81 nm) in contrast to WA. Overall, the treatment of NaOH/Na_2SO_3 and H_2O_2 achieved the removal of lignin and hemicellulose followed with larger surface area and porosity, providing a more desired condition for MIL-100(Fe) loading and contact with pollutions.

Table 1
Structural parameters of Wood, WA, MIL-100(Fe)/WA and MIL-100(Fe).

Samples	BET surface area[a] ($m^2\ g^{-1}$)	Pore size[b] (nm)	V_t[c] ($cm^3\ g^{-1}$)
Wood	6.19	4.15	0.0055
WA	8.77	6.10	0.0113
MIL-100(Fe)/WA	10.38	5.81	0.0169
MIL-100(Fe)	764.8	2.49	0.4062

[a] Determined by N_2 adsorption adopting Brunauer-Emmett-Teller (BET) method.
[b] Calculated from the desorption data employing Barrett-Joyner-Halenda (BJH) method.
[c] Total pore volume measured at $P/P_0 = 0.99$.

3.2. Catalytic performance

Based on the above characterization analysis, it was concluded that the combination of NaOH/Na_2SO_3 and H_2O_2 could effectively remove lignin and hemicellulose of balsa wood, thereby enlarging the surface area and porosity of WA, which further provided a more desirable condition for MIL-100(Fe) loading and the subsequent TC removal during PDS activation. As presented in Fig. 3a, it could be seen that PDS alone hardly removed TC with a slow degradation kinetic constant (k = 0.0004 $L{\cdot}mg^{-1}{\cdot}min^{-1}$) by second-order kinetic modern (Fig. 3b). So it was the same with WA, by which only a small fraction of TC was degraded (k = 0.0012 $L{\cdot}mg^{-1}{\cdot}min^{-1}$). The result suggested the poor degradation performance of PDS and WA. When MIL-100(Fe) in-situ grew on the channels of WA, the degradation efficiency of TC improved significantly by virtue of a high k of 0.0520 $L{\cdot}mg^{-1}{\cdot}min^{-1}$. At the meantime, contrasting to MIL-100(Fe)/wood, more TC was eliminated in MIL-100(Fe)/WA-PDS system, whose kinetic constant was 6.19 times that of MIL-100(Fe)/wood (0.0084 $L{\cdot}mg^{-1}{\cdot}min^{-1}$). This noticeable enhancement in TC degradation could be attributed to the improved structural performance with large surface area and porosity. Hence, the WA with a highly porous structure and open channels anchored with catalytic MIL-100(Fe) were able to eliminate TC efficiently, and the corresponding removal efficiency of total organic carbon (TOC) reflecting the total content (as carbon) of organic matter in water reached 64.01%, indicating the effective mineralization of TC in MIL-100(Fe)/WA-PDS system.

3.2.1. Influence factors

The catalytic performance in persulfate activation depended on many variables, such as PDS concentration, pH, and co-existing anions, which were investigated next.

In Fig. S2, with the increase in PDS concentration from 0.1 g L^{-1} to 0.3 g L^{-1}, the degradation efficiency towards TC enhanced, since more PDS were excited related to more $SO_4^{\cdot-}$, $OH^{\cdot}$ and related reactive species to degrade TC. While, with a high concentration of PDS (0.4 g L^{-1}), removal rate of TC did not increase further with a tiny drop. This indicated that a higher concentration of PDS was not conducive to TC degradation attributed to the saturated active site and the self-quenching effect of radicals [28], which could also be reflected by the decreased kinetic constant in the inserted image of Fig. S2.

In various factors, pH occupied a vital role in catalytic performance. As suggested in Fig. 3c, it was obvious that MIL-100(Fe)/WA-PDS system behaved satisfyingly with high TC removal at the initial pH range of 2–8, in which the TC removal efficiency was the best at the pH of 4. When the initial pH reached to 10, a clear reduction in TC degradation was observed. Correspondingly, their relative kinetics constant accorded with the degradation tendency as shown in Fig. 3d. It was seen that the k at pH of 10 decreased to 0.0230 $L{\cdot}mg^{-1}{\cdot}min^{-1}$ compared with other conditions. The enhanced inhibiting effect at higher pH could be ascribed to the abundant OH^- in the solution combined with active Fe sites of MIL-100(Fe)/WA, thus weakening the activation of PDS to produce reactive species. Meanwhile, considering the amphoterism of TC with different dissociation constants (pKa: 3.32, 7.78 and 9.58) [29], the changed forms of TC would not affect the TC degradation in MIL-100 (Fe)/WA-PDS system.

Given the complexity of real wastewater, co-existing ion is another important part that affects pollution removal in AOPs, especially the inhibition of anions [30]. Therefore, the effect of various anions (Cl^-, SO_4^{2-}, HCO_3^-, CO_3^{2-} and PO_4^{3-}) on TC elimination in MIL-100(Fe) /WA-PDS system was conducted. With the addition of 1 mM anions, the result

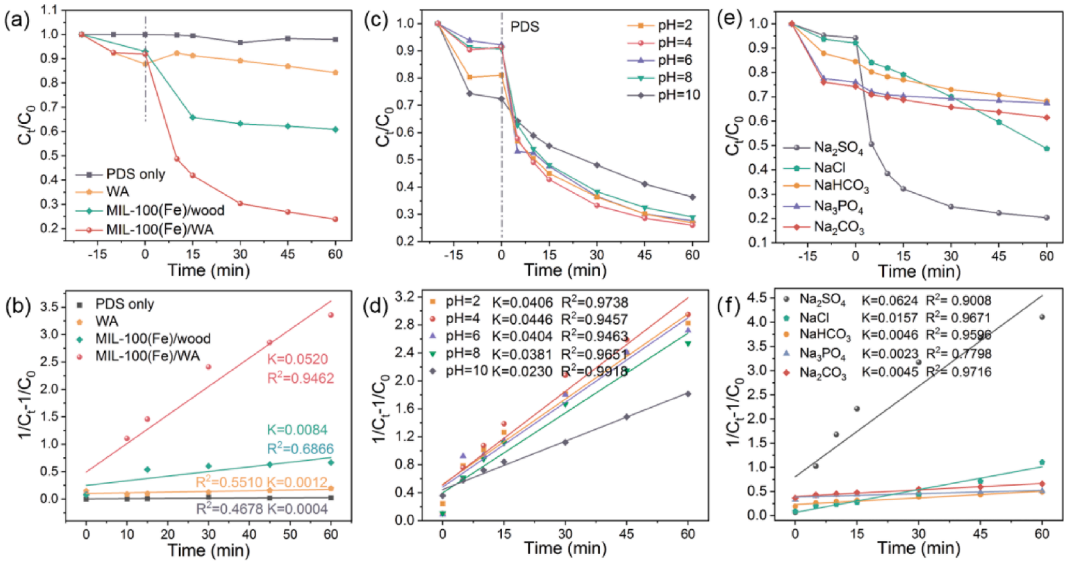

Fig. 3. The degradation efficiency of different systems (a) and their kinetic constants ($L{\cdot}mg^{-1}{\cdot}min^{-1}$) (b); the effect of initial pH (c) and their kinetic constants (d); the effect of various anions (e) and their kinetic constants (f). Condition: TC = 30 mg L^{-1}, pH = 4.40, T = 298 K, PDS = 0.3 g L^{-1}

presented in Fig. 3e revealed that except for SO_4^{2-} without inhibition effect, other anions resulted in a prominent suppression in TC degradation, and the corresponding kinetic constants (Fig. 3f) decreased to 0.0157 (Cl^-), 0.0046 (HCO_3^-), 0.0045 (CO_3^{2-}), and 0.0023 $L{\cdot}mg^{-1}{\cdot}min^{-1}$ (PO_4^{3-}), respectively. Meanwhile, a different degradation process was seen in Cl^- induced process, where TC was slowly degraded as time went by. The phenomenon could be caused by the reaction between Cl^- and $SO_4^{\bullet-}$ or $^{\bullet}OH$ resulting in the generation of $ClOH^{\bullet-}$ ($E^0 = 1.8$ V), $Cl_2^{\bullet-}$ ($E^0 = 2.1$ V) and $Cl^{\bullet}$ ($E^0 = 2.5$ V) with low redox potential to further oxide TC according to the Eqs (1–3) [31]. As for HCO_3^- and CO_3^{2-}, their similar suppression towards TC degradation resulted from their interaction with $SO_4^{\bullet-}$ or $^{\bullet}OH$ [32], as well as their hydrolysis, leading to the increase of solution pH, which decreased TC removal. Regarding PO_4^{3-}, it is reported that PO_4^{3-} could form complexes with the metal on the catalyst, as well as the quenching effect on radicals [33]. Thus, the coexistence of PO_4^{3-} would hinder the function of active sites on MIL-100(Fe)/WA.

$$SO_4^{\bullet-} + Cl^- \rightarrow SO_4^{2-} + Cl^{\bullet} \quad (1)$$

$$Cl^{\bullet} + Cl^- \rightarrow Cl_2^{\bullet-} \quad (2)$$

$$^{\bullet}OH + Cl^- \rightarrow ClOH^{\bullet-} \quad (3)$$

Besides the above factors, the reaction temperature was another important variable in AOPs. With the increase in temperature, it could be seen that the efficiency towards TC degradation enhanced, suggesting that elevated temperature facilitated TC degradation by MIL-100(Fe)/WA-PDS system (Fig. S3a). This was caused by the reason that high reaction temperature accelerated the activation of PDS through the break of O-O, achieving more TC removed. Further, according to the kinetic constant at different temperatures, the Arrhenius model was employed for calculating the activation energy during the catalytic process [34]:

$$\ln(k) = -E_A/RT + \ln(A) \quad (4)$$

at which k and E_A (kJ mol^{-1}) were kinetic constant and activation energy, T (K) and R (8.314 J mol^{-1} K^{-1}) denoted temperature and gas constant, A referred to pre-exponential factors.

As described in Fig. S3b, the high R^2 (0.9828) suggested the credible fitting result, and the obtained E_A was around 20.31 kJ mol^{-1}. The calculated E_A meant that TC oxidization by MIL-100(Fe)/WA-PDS system required moderate energy and was easy to happen [35], attributed to the enlarged open porous structure with accessible active sites, which could be regarded as a diffusion-controlled reaction [36].

3.3. Catalytic mechanism

To identify the reactive oxygen species participating in the PDS activation, quenching experiments aimed at $SO_4^{\bullet-}$, $^{\bullet}OH$, $O_2^{\bullet-}$, and $^1O_2$ which employed MeOH, TBA, BQ, and NaN_3 as quenching agents were carried out [37]. Fig. 4a manifested the influence of different quenching agents compared with the blank control trial. It was clear that the presence of MeOH and TBA (25 mM) had no obvious impact on TC removal, while BQ and NaN_3 showed a significant suppression effect due to their low TC degradation efficiency in MIL-100(Fe)/WA-PDS system. Accordingly, their kinetic constants (Fig. 4b) drooped to 0.0146 $L{\cdot}mg^{-1}{\cdot}min^{-1}$ (BQ) and 0.0030 $L{\cdot}mg^{-1}{\cdot}min^{-1}$ (NaN_3). This result suggested that $O_2^{\bullet-}$ and $^1O_2$ produced in the catalysis process were quenched by BQ and NaN_3 effectively [38], and $O_2^{\bullet-}$ and $^1O_2$ played a significant role in TC oxidation and degradation. Further, considering the quenching experiments using low concentration of scavengers aiming at free ROS, DMSO (dimethyl sulfoxide) and high concentration of MeOH and TBA were used to quench surface-bound radicals [39]. As shown in Fig. S5, the addition of DMSO (2 mM), MeOH (50 mM) and TBA (50 mM) had significant inhibiting effects on TC removal, indicating the effective participation of surface-bound radicals ($SO_4^{\bullet-}$, $^{\bullet}OH$) in TC degradation. Therefore, surface-bound radicals ($SO_4^{\bullet-}$, $^{\bullet}OH$) also made a contribution to TC degradation. As a result, TC removal in MIL-100(Fe)/WA-PDS system was attributed to the surface-bound radicals ($SO_4^{\bullet-}$, $^{\bullet}OH$), $O_2^{\bullet-}$ and $^1O_2$.

Based on the quenching experiments, for further proving the existence of $O_2^{\bullet-}$ and $^1O_2$ in MIL-100(Fe)/WA-PDS system, EPR (Electron Paramagnetic Resonance) was utilized to in-situ recognize the two ROS [40]. TEMP and DMPO were used as the corresponding spin-trapping agents for $^1O_2$ and $O_2^{\bullet-}$ [41]. For $O_2^{\bullet-}$ in Fig. 4c, there was no signal in the PDS system. As MIL-100(Fe)/WA was added into the PDS system, the typical signal of DMPO-$O_2^{\bullet-}$ adducts emerged, suggesting the presence of $O_2^{\bullet-}$ in this activation system [42]. Besides, it was the same condition as $^1O_2$. As MIL-100(Fe)/WA was added, the signal belonging to TEMP-$^1O_2$ adducts appeared compared with PDS system in Fig. 4d, which mean that $^1O_2$ participated in TC degradation. The above analysis of EPR conformed to the presence of $^1O_2$ and $O_2^{\bullet-}$ in PDS activation process, which also accorded with the result of quenching experiments. Therefore, $^1O_2$ and $O_2^{\bullet-}$ were recognized as significant ROS in TC degradation.

Moreover, the element variation in composition and valence before and after TC degradation by XPS was monitored. As presented in Fig. 4e, the binding energy of Fe after the catalysis reaction shifted to a higher

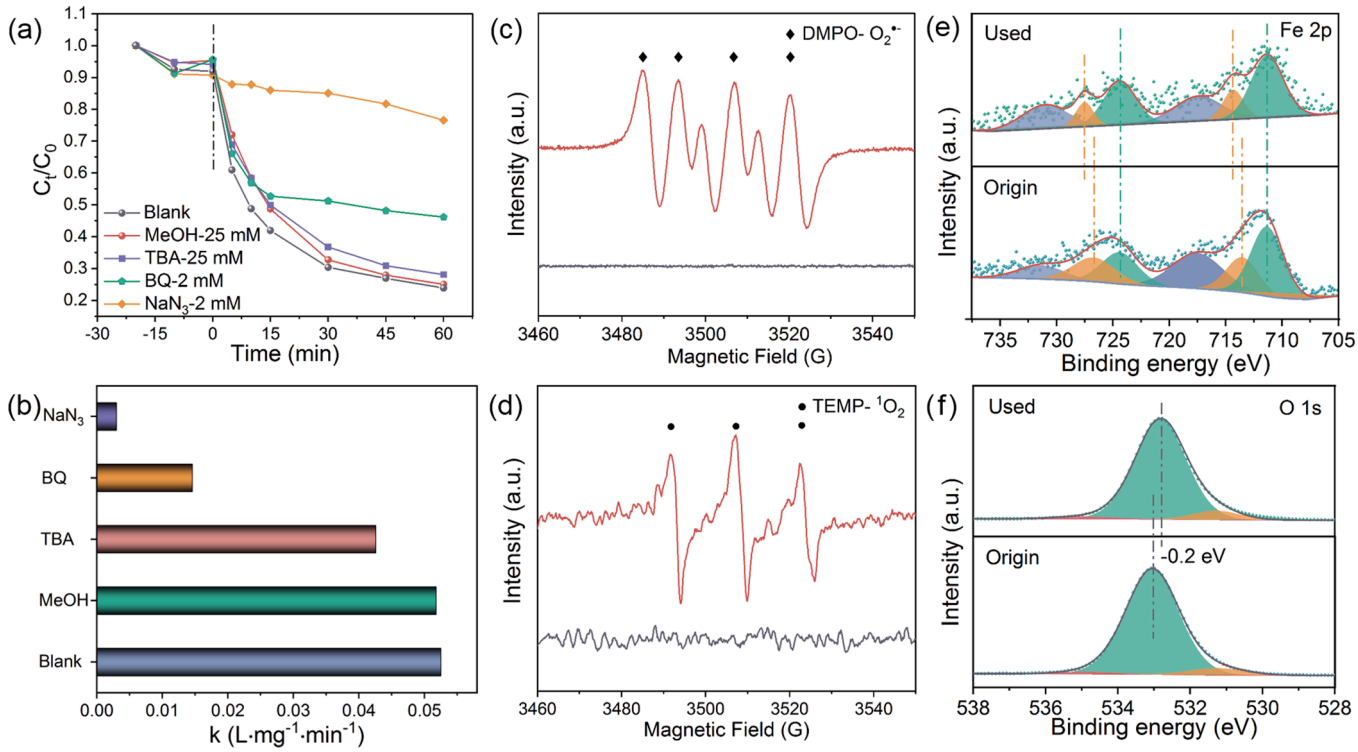

Fig. 4. Quenching experiments (a) and the corresponding kinetic constants (b); EPR of DMPO-$O_2^{\bullet-}$ (c) and TEMP-$^1O_2$ (d); Fe 2p (e) and O 1 s (f) of origin and used MIL-100(Fe)/WA. Condition: TC = 30 mg L^{-1}, pH = 4.40, T = 298 K, PDS = 0.3 g L^{-1}

level compared with the origin state, while the O shifted to a lower binding energy (Fig. 4f). The shifted binding energy indicated the electron transfer and their participation in PDS exciting [43]. It could be seen that the proportion of Fe(III) decreased from 37.76% to 25.22%, meanwhile the proportion of Fe(II) varied from 62.24% to 74.78%. The ≡Fe(II) in the catalyst could react with $S_2O_8^{2-}$ to generate $SO_4^{\bullet-}$ and ≡Fe (III) which would consume $S_2O_8^{2-}$ to form ≡Fe(II) (Eqs 5–6). The form and conversion of Fe(II)/Fe(III) cycle continued to activate PDS for TC degradation. At the same time, $S_2O_8^{2-}$ could be converted into SO_4^{2-} and HO_2^- that further reacted with $S_2O_8^{2-}$ or underwent transformation to form $O_2^{\bullet-}$ (Eqs 7–9). To verify the effect of O_2 which could involve in $O_2^{\bullet-}$ generation (Eq 10) [44], TC degradation in N_2 and O_2 condition was conducted. The result in Fig. S4 suggested that there was no obvious impact on TC removal, which meant the O_2 had no effect on $O_2^{\bullet-}$ generation. Typically, $^1O_2$ generated in the PDS activation was attributed to the conversation of $O_2^{\bullet-}$ under the acidic condition with abundant H^+ according to Eq (11) [45]. On the other hand, $^1O_2$ could be derived from the disproportionation reaction of produced $^{\bullet}OH$ in the activation system (Eqs 12–13) [46]. In this way, TC degradation in MIL-100(Fe)/WA-PDS system mainly depended on the contribution of $O_2^{\bullet-}$, $^1O_2$ and surface-

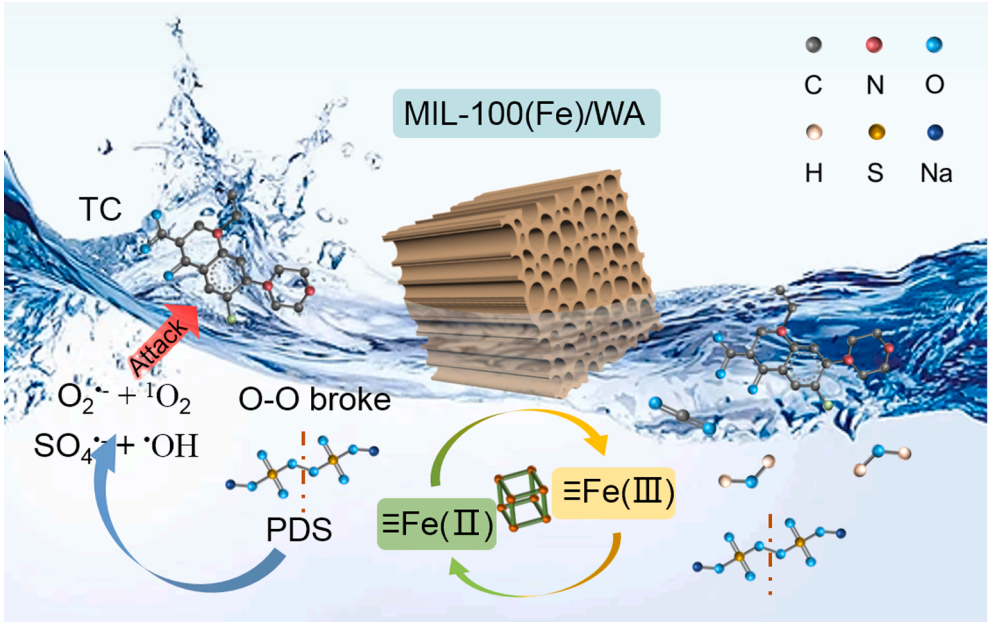

Fig. 5. The proposed TC degradation mechanism in MIL-100(Fe)/WA-PDS system.

bound radicals ($SO_4^{\bullet-}$, $^{\bullet}OH$) as described in Fig. 5.

$$\equiv Fe(II) + S_2O_8^{2-} \rightarrow \equiv Fe(III) + SO_4^{2-} + SO_4^{\bullet-} \quad (5)$$

$$\equiv Fe(III) + S_2O_8^{2-} \rightarrow \equiv Fe(II) + S_2O_8^{\bullet-} \quad (6)$$

$$S_2O_8^{2-} + H_2O \rightarrow 2SO_4^{2-} + HO_2^- + H^+ \quad (7)$$

$$S_2O_8^{2-} + HO_2^- \rightarrow SO_4^{\bullet-} + SO_4^{2-} + O_2^{\bullet-} + H^+ \quad (8)$$

$$HO_2^- \rightarrow H^+ + O_2^{\bullet-} \quad (9)$$

$$O_2^{\bullet-} + H^+ \rightarrow {}^1O_2 + H_2O_2 \quad (10)$$

$$Fe^{2+} + O_2 \rightarrow Fe^{3+} + O_2^{\bullet-} \quad (11)$$

$$SO_4^{\bullet-} + H_2O \rightarrow SO_4^{2-} + {}^{\bullet}OH + H^+ \quad (12)$$

$$^{\bullet}OH + {}^{\bullet}OH \rightarrow {}^1O_2 + H_2O \quad (13)$$

3.4. Possible degradation pathways

According to the catalytic process, intermediate oxidation by-products of TC in the MIL-100(Fe)/WA-PDS system which were presented in Fig. S6, were recognized by employing LC-MS technology. The origin TC sample displayed a sharp MS signal located in m/z = 445, belonging to TC molecules. Depending on the by-products of TC oxidation (P1-P10), a possible TC degradation pathway was proposed as described in Fig. 6. It was reported that TC degradation was mainly involved in hydroxyl addition, deamination, demethylation, and ring opening [47]. Firstly, the break of C-N by ROS could lead to the separation of methyl to form P1 (m/z = 417). On the other hand, the loss of hydroxyl resulted in the form of P2 (m/z = 427). The produced P1 and P2 could be transferred into P3 (m/z = 397) through deamination and demethylation. Further, the loss of methyl, hydroxyl and the following ring opening formed P4 (m/z = 362), P5 (m/z = 318) and P6 (m/z = 302). P6 was oxidized into P7 (m/z = 284), P8 (m/z = 274), P9 (m/z = 246), and P10 (m/z = 194) under the attack of ROS generated in MIL-100(Fe)/WA-PDS system. Ultimately, P10 was further degraded into small molecules, CO_2, and H_2O, as evidenced by the TOC removal efficiency (64.01%), thus achieving the TC degradation.

3.5. Recyclability, stability and other antibiotics degradation

For practical application, recyclability was regarded as an essential part of the potential of persulfate-based AOPs. Fig. 7a displayed the cycle performance of MIL-100(Fe)/WA. As observed, after the fifth use, the degradation efficiency of TC did not decrease significantly, indicating the acceptable regeneration capacity of MIL-100(Fe)/WA originating from its high open porous structure with accessible catalytic sites. Due to the untargeted attack of produced ROS, the released Fe (0.125 mg, from the result of ICP-MS) and carbon (1.74 mg, from the increased TOC) which could be from MIL-100(Fe) and wood aerogel was detected. Hence, the dropped catalytic ability could be linked to the breaking of active Fe sites reflected by XPS analysis (Fig. 4e and Table S2). Regarding the stability, as shown in Fig. 7b, similar XRD diffraction of

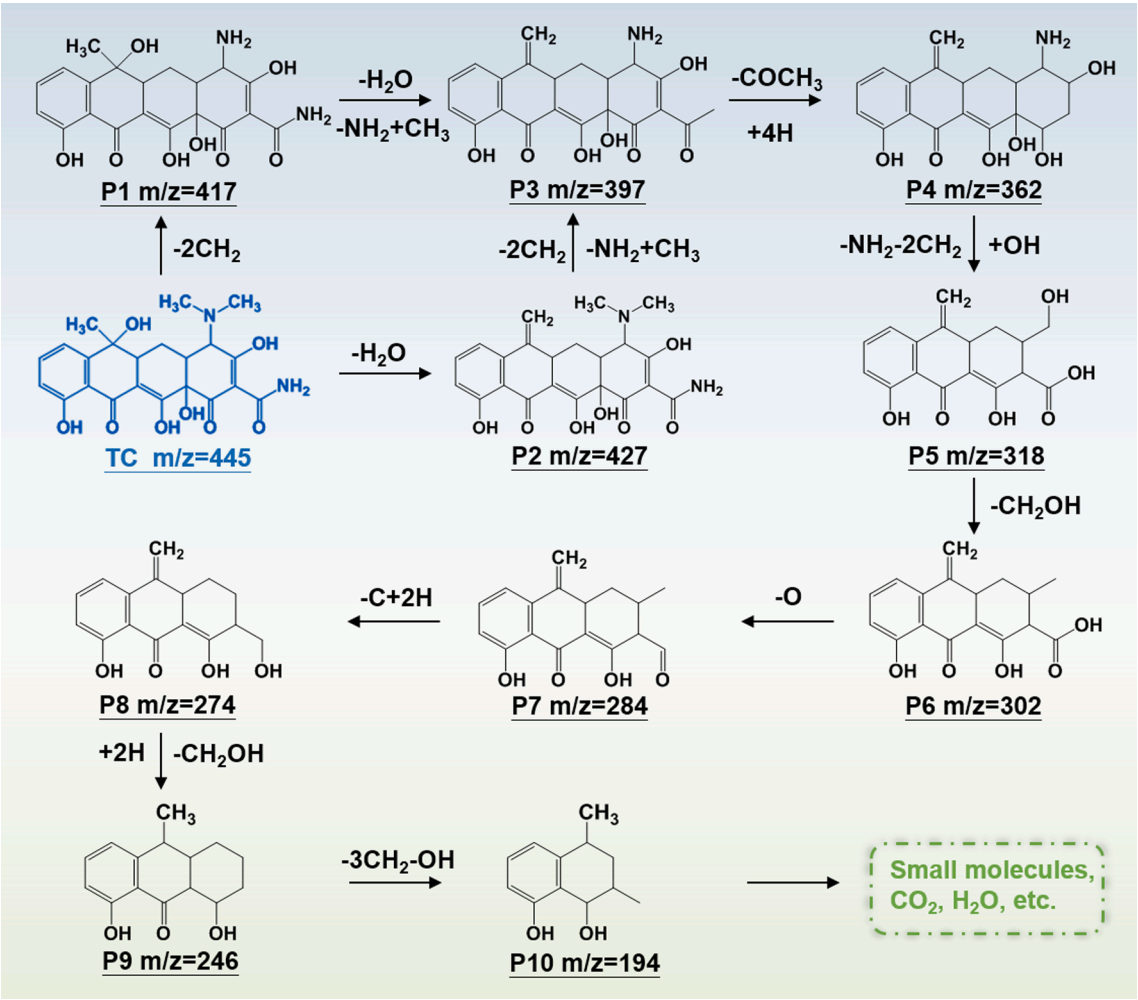

Fig. 6. The proposed degradation pathway of TC in MIL-100(Fe)/WA-PDS system.

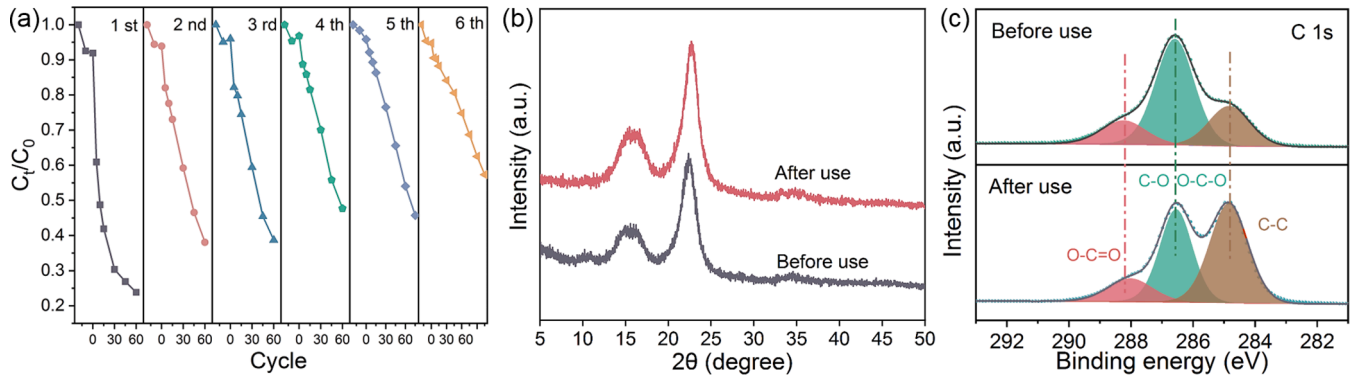

Fig. 7. The recyclability of MIL-100(Fe)/WA (a). (Condition: TC = 30 mg L^{-1}, pH = 4.40, T = 298 K, PDS = 0.3 g L^{-1}); XRD pattern (b) and C 1 s (c) of MIL-100(Fe)/WA before and after use.

MIL-100(Fe)/WA before and after use indicated the stability of MIL-100(Fe)/WA in certain degree. Besides, the content of C-O/O-C-O decreased distinctly from 59.9% to 38.4% (Fig. 7c), suggesting the partial break of C-O/O-C-O from MIL-100(Fe) (trimesic acid linker) and WA (cellulose/hemicellulose) due to attack of ROS. Overall, the untargeted attack of produced ROS in PDS activation would lead to a reduced performance in stability, coupled with weaken reusability.

Meanwhile, towards other antibiotics such as chlortetracycline and oxytetracycline, MIL-100(Fe)/WA-PDS system was able to perform well in their removal (Fig. S7a). Besides, different water matrixes for simulating TC removal were carried out. As shown in Fig. S6c, compared with the control group, TC removal efficiency decreased obviously. The reduced performance was mainly caused by the presence of co-existing ions such as Cl^- and CO_3^{2-} based on the effect of anions, as well as the dissolved organic matter reflected by the TOC (Table S4).

4. Conclusion

Herein, MIL-100(Fe) functionalized porous wood aerogel composites (MIL-100(Fe)/WA) were prepared via combining pretreatment, solvothermal synthesis, and freeze drying. Considering the limited porosity in original wood supports, pretreatment with Na_2SO_3/NaOH and H_2O_2 enabled to partially remove lignin and hemicellulose of cellular structures in wood effectively, turning wood into wood aerogel, which largely improved the porosity (from 0.0055 to 0.0113 $cm^3\ g^{-1}$) and surface area (from 6.19 to 8.77 $m^2\ g^{-1}$) as well as pore size (Table 1). The enlarged open porous channels in WA supplied the desired growing condition for MIL-100(Fe) anchoring. Accordingly, the fabricated MIL-100(Fe)/WA exhibited faster and more efficient degradation capacity of TC through PDS activation compared with MIL-100(Fe)/wood, of which its corresponding kinetic constant (0.0520 $L{\cdot}mg^{-1}{\cdot}min^{-1}$) was 6.19 times that of MIL-100(Fe)/wood (0.0084 $L{\cdot}mg^{-1}{\cdot}min^{-1}$). The translation between ≡Fe(II) and ≡Fe(III) and the participation of O proved by XPS analysis contributed to the PDS exciting. Mechanism investigation by quenching tests and EPR analysis further made clear that $O_2^{\cdot-}$, $^1O_2$ and surface-bound radicals ($SO_4^{\cdot-}$, $^{\cdot}OH$) ere the dominating ROS for TC degradation in MIL-100(Fe)/WA-PDS oxidative system. Besides, it was found that TC removal by MIL-100(Fe)/WA-PDS system was a temperate-promoting process with low activation energy, and could be conducted in a wide pH range (2–10). Regeneration experiments with acceptable dropped performance after the fourth reuse and satisfactory removal efficiency towards other antibiotics suggested its application potential. Based on the low-prize and renewable wood, this work functionalized wood aerogel with MIL-100(Fe) to effectively eliminate antibiotics by persulfate activation, which might supply an accessible approach for designing MOFs-based material in water treatment.

CRediT authorship contribution statement

Haihao Peng: Data curation, Writing – original draft. **Jing Tong:** Data curation, Writing – review & editing. **Jing Huang:** Supervision, Funding acquisition. **Zhaohui Yang:** Supervision, Funding acquisition. **Weiping Xiong:** Funding acquisition, Writing – review & editing. **Yuxuan Yao:** Writing – review & editing. **Yinping Xiang:** Writing – review & editing. **Zhengyong Xu:** Writing – review & editing.

Declaration of Competing Interest

The authors declare that they have no known competing financial interests or personal relationships that could have appeared to influence the work reported in this paper.

Data availability

Data will be made available on request.

Acknowledgements

The study was financially supported by the Special Funding for the Construction of Hunan's Innovative Province (2021SK2040), the National Youth Foundation of China (52000064) and the Science and Technology Innovation Program of Hunan Province (2021RC3133).

Appendix A. Supplementary data

Supplementary data to this article can be found online at https://doi.org/10.1016/j.seppur.2023.124195.

References

[1] Z. Yu, H. Rabiee, J. Guo, Synergistic effect of sulfidated nano zerovalent iron and persulfate on inactivating antibiotic resistant bacteria and antibiotic resistance genes, Water Res. 198 (2021), 117141, https://doi.org/10.1016/j.watres.2021.117141.

[2] D.B. Miklos, C. Remy, M. Jekel, K.G. Linden, J.E. Drewes, U. Hubner, Evaluation of advanced oxidation processes for water and wastewater treatment - A critical review, Water Res. 139 (2018) 118–131, https://doi.org/10.1016/j.watres.2018.03.042.

[3] W. Tang, Y. Dai, K.H. Row, Evaluation of fatty acid/alcohol-based hydrophobic deep eutectic solvents as media for extracting antibiotics from environmental water, Anal. Bioanal. Chem. 410 (28) (2018) 7325–7336, https://doi.org/10.1007/s00216-018-1346-6.

[4] J. Lee, U. von Gunten, J.H. Kim, Persulfate-based advanced oxidation: critical assessment of opportunities and roadblocks, Environ. Sci. Tech. 54 (6) (2020) 3064–3081, https://doi.org/10.1021/acs.est.9b07082.

[5] H. Peng, W. Xiong, Z. Yang, J. Tong, M. Jia, Y. Xiang, S. Sun, Z. Xu, Fe_3O_4-supported N-doped carbon channels in wood carbon form etching and carbonization: Boosting performance for persulfate activating, Chem. Eng. J. 457 (2023) 141317, https://doi.org/10.1016/j.cej.2023.141317.

[6] W. Ren, C. Cheng, P. Shao, X. Luo, H. Zhang, S. Wang, X. Duan, Origins of electron-transfer regime in persulfate-based nonradical oxidation processes, Environ. Sci. Tech. 56 (1) (2022) 78–97, https://doi.org/10.1021/acs.est.1c05374.

[7] H. Peng, W. Xiong, Z. Yang, Z. Xu, J. Cao, M. Jia, Y. Xiang, Advanced MOFs@ aerogel composites: Construction and application towards environmental remediation, J. Hazard. Mater. 432 (2022), 128684, https://doi.org/10.1016/j.jhazmat.2022.128684.

[8] J. Garemark, X. Yang, X. Sheng, O. Cheung, L. Sun, L.A. Berglund, Y. Li, Top-down approach making anisotropic cellulose aerogels as universal substrates for multifunctionalization, ACS Nano 14 (6) (2020) 7111–7120, https://doi.org/10.1021/acsnano.0c01888.

[9] Y. Lu, D. Fan, Z. Shen, H. Zhang, H. Xu, X. Yang, Design and performance boost of a MOF-functionalized-wood solar evaporator through tuning the hydrogen-bonding interactions, Nano Energy 95 (2022), 107016, https://doi.org/10.1016/j.nanoen.2022.107016.

[10] K. Tu, S. Buchele, S. Mitchell, L. Stricker, C. Liu, C. Goldhahn, J. Allaz, Y. Ding, R. Gunther, Z. Zhang, J. Sun, S. Stucki, G. Panzarasa, S.C. Zeeman, I. Burgert, J. Perez-Ramirez, T. Keplinger, Natural wood-based catalytic membrane microreactors for continuous hydrogen generation, ACS Appl Mater Inter 14 (6) (2022) 8417–8426, https://doi.org/10.1021/acsami.1c22850.

[11] R. Guo, X. Cai, H. Liu, Z. Yang, Y. Meng, F. Chen, Y. Li, B. Wang, In situ growth of metal-organic frameworks in three-dimensional aligned lumen arrays of wood for rapid and highly efficient organic pollutant removal, Environ. Sci. Tech. 53 (5) (2019) 2705–2712, https://doi.org/10.1021/acs.est.8b06564.

[12] Y. Gu, Y. Wang, H. Li, W. Qin, H. Zhang, G. Wang, Y. Zhang, H. Zhao, Fabrication of hierarchically porous NH_2-MIL-53/wood-carbon hybrid membrane for highly effective and selective sequestration of Pb^{2+}, Chem. Eng. J. 387 (2020), 124141 https://doi.org/10.1016/j.cej.2020.124141.

[13] X.-F. Zhang, Z. Wang, L. Song, J. Yao, In situ growth of ZIF-8 within wood channels for water pollutants removal, Sep. Purif. Technol. 266 (2021), 118527, https://doi.org/10.1016/j.seppur.2021.118527.

[14] J. Song, C. Chen, Z. Yang, Y. Kuang, T. Li, Y. Li, H. Huang, I. Kierzewski, B. Liu, S. He, T. Gao, S.U. Yuruker, A. Gong, B. Yang, L. Hu, Highly compressible, anisotropic aerogel with aligned cellulose nanofibers, ACS Nano 12 (1) (2018) 140–147, https://doi.org/10.1021/acsnano.7b04246.

[15] X. Ma, Y. Xiong, Y. Liu, J. Han, G. Duan, Y. Chen, S. He, C. Mei, S. Jiang, K. Zhang, When MOFs meet wood: From opportunities toward applications, Chem 8 (9) (2022) 2342–2361, https://doi.org/10.1016/j.chempr.2022.06.016.

[16] H. Guan, Z. Cheng, X. Wang, Highly compressible wood sponges with a spring-like lamellar structure as effective and reusable oil absorbents, ACS Nano 12 (10) (2018) 10365–10373, https://doi.org/10.1021/acsnano.8b05763.

[17] K. Wang, X. Liu, Y. Tan, W. Zhang, S. Zhang, J. Li, Two-dimensional membrane and three-dimensional bulk aerogel materials via top-down wood nanotechnology for multibehavioral and reusable oil/water separation, Chem. Eng. J. 371 (2019) 769–780, https://doi.org/10.1016/j.cej.2019.04.108.

[18] G. Chen, S. He, G. Shi, Y. Ma, C. Ruan, X. Jin, Q. Chen, X. Liu, H. Dai, X. Chen, D. Huang, In-situ immobilization of ZIF-67 on wood aerogel for effective removal of tetracycline from water, Chem. Eng. J. 423 (2021), 130184, https://doi.org/10.1016/j.cej.2021.130184.

[19] T. Liu, X. Zhang, A. Gu, Y. Liu, M. Chen, H. Wang, R. Zhang, S. Tang, Z. Xie, N. Wang, In-situ grown bilayer MOF from robust wood aerogel with aligned microchannel arrays toward selective extraction of uranium from seawater, Chem. Eng. J. 433 (2022), 134346, https://doi.org/10.1016/j.cej.2021.134346.

[20] Y. Wan, J. Wang, F. Huang, Y. Xue, N. Cai, J. Liu, W. Chen, F. Yu, Synergistic effect of adsorption coupled with catalysis based on graphene-supported MOF hybrid aerogel for promoted removal of dyes, RSC Adv. 8 (60) (2018) 34552–34559, https://doi.org/10.1039/c8ra05873c.

[21] M.-J. Chang, W.-N. Cui, X.-J. Chai, J. Liu, K. Wang, L. Qiu, Fabrication of flexible MIL-100(Fe) supported SiO_2 nanofibrous membrane for visible light photocatalysis, J. Mater. Sci. Mater. Electron. 30 (2) (2018) 1009–1016, https://doi.org/10.1007/s10854-018-0370-9.

[22] G. Chen, T. Li, C. Chen, W. Kong, M. Jiao, B. Jiang, Q. Xia, Z. Liang, Y. Liu, S. He, L. Hu, Scalable wood hydrogel membrane with nanoscale channels, ACS Nano 15 (2021) 11244–11252, https://doi.org/10.1021/acsnano.0c10117.

[23] J. Tang, J. Wang, Metal organic framework with coordinatively unsaturated sites as efficient fenton-like catalyst for enhanced degradation of sulfamethazine, Environ. Sci. Tech. 52 (9) (2018) 5367–5377, https://doi.org/10.1021/acs.est.8b00092.

[24] M. Nehra, N. Dilbaghi, N.K. Singhal, A.A. Hassan, K.H. Kim, S. Kumar, Metal organic frameworks MIL-100(Fe) as an efficient adsorptive material for phosphate management, Environ. Res. 169 (2019) 229–236, https://doi.org/10.1016/j.envres.2018.11.013.

[25] T. Meng, B. Jiang, Z. Li, X. Xu, D. Li, J. Henzie, A.K. Nanjundan, Y. Yamauchi, Y. Bando, Programmed design of selectively-functionalized wood aerogel: Affordable and mildew-resistant solar-driven evaporator, Nano Energy 87 (2021), 106146, https://doi.org/10.1016/j.nanoen.2021.106146.

[26] P. Song, H. Xu, S. Sun, W. Xiong, Z. Yang, Remediation of arsenic-spiked soil by biochar-loaded nanoscale zero-valent iron: Performance, mechanism, and microbial response, J. Clean. Prod. 380 (2022), https://doi.org/10.1016/j.jclepro.2022.134985.

[27] H. Peng, W. Xiong, Z. Yang, J. Cao, M. Jia, Y. Xiang, Q. Hu, Z. Xu, Facile fabrication of three-dimensional hierarchical porous ZIF-L/gelatin aerogel: Highly efficient adsorbent with excellent recyclability towards antibiotics, Chem. Eng. J. 426 (2021), 130798, https://doi.org/10.1016/j.cej.2021.130798.

[28] Y. Jing, M. Jia, Z. Xu, W. Xiong, Z. Yang, H. Peng, J. Cao, Y. Xiang, C. Zhang, Facile synthesis of recyclable 3D gelatin aerogel decorated with MIL-88B(Fe) for activation peroxydisulfate degradation of norfloxacin, J. Hazard. Mater. 424 (424) (2021), 127503, https://doi.org/10.1016/j.jhazmat.2021.127503.

[29] H. Peng, J. Cao, W. Xiong, Z. Yang, M. Jia, S. Sun, Z. Xu, Y. Zhang, H. Cai, Two-dimension N-doped nanoporous carbon from KCl thermal exfoliation of Zn-ZIF-L: Efficient adsorption for tetracycline and optimizing of response surface model, J. Hazard. Mater. 402 (2021), 123498, https://doi.org/10.1016/j.jhazmat.2020.123498.

[30] Y. Li, H. Dong, L. Li, J. Xiao, S. Xiao, Z. Jin, Efficient degradation of sulfamethazine via activation of percarbonate by chalcopyrite, Water Res. 202 (2021), 117451, https://doi.org/10.1016/j.watres.2021.117451.

[31] N. Li, R. Li, X. Duan, B. Yan, W. Liu, Z. Cheng, G. Chen, L. Hou, S. Wang, Correlation of active sites to generated reactive species and degradation routes of organics in peroxymonosulfate activation by Co-loaded carbon, Environ. Sci. Tech. 55 (23) (2021) 16163–16174, https://doi.org/10.1021/acs.est.1c06244.

[32] W. Qin, Y. Gu, G. Wang, T. Wu, H. Zhang, X. Tang, Y. Zhang, H. Zhao, Zirconium metal organic frameworks-based DGT technique for in situ measurement of dissolved reactive phosphorus in waters, Water Res. 147 (2018) 223–232, https://doi.org/10.1016/j.watres.2018.10.003.

[33] N. Li, Y. Wang, X. Cheng, H. Dai, B. Yan, G. Chen, L. Hou, S. Wang, Influences and mechanisms of phosphate ions onto persulfate activation and organic degradation in water treatment: A review, Water Res. 222 (2022), 118896, https://doi.org/10.1016/j.watres.2022.118896.

[34] Y. Ji, Y. Fan, K. Liu, D. Kong, J. Lu, Thermo activated persulfate oxidation of antibiotic sulfamethoxazole and structurally related compounds, Water Res. 87 (2015) 1–9, https://doi.org/10.1016/j.watres.2015.09.005.

[35] A. Ghauch, A.M. Tuqan, N. Kibbi, Naproxen abatement by thermally activated persulfate in aqueous systems, Chem. Eng. J. 279 (2015) 861–873, https://doi.org/10.1016/j.cej.2015.05.067.

[36] Y. Feng, J. Liu, D. Wu, Z. Zhou, Y. Deng, T. Zhang, K. Shih, Efficient degradation of sulfamethazine with $CuCo_2O_4$ spinel nanocatalysts for peroxymonosulfate activation, Chem. Eng. J. 280 (2015) 514–524, https://doi.org/10.1016/j.cej.2015.05.121.

[37] J. Tong, L. Chen, J. Cao, Z. Yang, W. Xiong, M. Jia, Y. Xiang, H. Peng, Biochar supported magnetic MIL-53-Fe derivatives as an efficient catalyst for peroxydisulfate activation towards antibiotics degradation, Sep. Purif. Technol. 294 (2022), 121064, https://doi.org/10.1016/j.seppur.2022.121064.

[38] X. Fan, Q. Lin, J. Zheng, H. Fu, K. Xu, Y. Liu, Y. Ma, J. He, Peroxydisulfate activation by nano zero-valent iron graphitized carbon materials for ciprofloxacin removal: Effects and mechanism, J. Hazard. Mater. 437 (2022), 129392, https://doi.org/10.1016/j.jhazmat.2022.129392.

[39] S. Zhu, X. Huang, F. Ma, L. Wang, X. Duan, S. Wang, Catalytic removal of aqueous contaminants on N-doped graphitic biochars: Inherent roles of adsorption and nonradical mechanisms, Environ. Sci. Tech. 52 (15) (2018) 8649–8658, https://doi.org/10.1021/acs.est.8b01817.

[40] Y. Zhen, S. Zhu, Z. Sun, Y. Tian, Z. Li, C. Yang, J. Ma, Identifying the Persistent Free Radicals (PFRs) Formed as Crucial Metastable Intermediates during Peroxymonosulfate (PMS) Activation by N-Doped Carbonaceous Materials, Environ. Sci. Tech. 55 (13) (2021) 9293–9304, https://doi.org/10.1021/acs.est.1c01974.

[41] G. Yu, Y. Wang, H. Cao, H. Zhao, Y. Xie, Reactive oxygen species and catalytic active sites in heterogeneous catalytic ozonation for water purification, Environ. Sci. Tech. 54 (10) (2020) 5931–5946, https://doi.org/10.1021/acs.est.0c00575.

[42] Y. Wang, J. Cao, Z. Yang, W. Xiong, Z. Xu, P. Song, M. Jia, S. Sun, Y. Zhang, W. Li, Fabricating iron-cobalt layered double hydroxide derived from metal-organic framework for the activation of peroxymonosulfate towards tetracycline degradation, J. Solid State Chem. 294 (2021), 121857, https://doi.org/10.1016/j.jssc.2020.121857.

[43] J. Cao, Z. Yang, W. Xiong, Y. Zhou, Y. Wu, M. Jia, H. Peng, Y. Yuan, Y. Xiang, C. Zhou, Three-dimensional MOF-derived hierarchically porous aerogels activate peroxymonosulfate for efficient organic pollutants removal, Chem. Eng. J. 427 (2022), 130830, https://doi.org/10.1016/j.cej.2021.130830.

[44] Y. Wu, X. Chen, Y. Han, D. Yue, X. Cao, Y. Zhao, X. Qian, Highly Efficient Utilization of Nano-Fe(0) Embedded in Mesoporous Carbon for Activation of Peroxydisulfate, Environ. Sci. Tech. 53 (15) (2019) 9081–9090, https://doi.org/10.1021/acs.est.9b02170.

[45] C. Ling, S. Wu, J. Han, T. Dong, C. Zhu, X. Li, L. Xu, Y. Zhang, M. Zhou, Y. Pan, Sulfide-modified zero-valent iron activated periodate for sulfadiazine removal: Performance and dominant routine of reactive species production, Water Res. 220 (2022), 118676, https://doi.org/10.1016/j.watres.2022.118676.

[46] B. Shen, C. Dong, J. Ji, M. Xing, J. Zhang, Efficient Fe(III)/Fe(II) cycling triggered by MoO_2 in Fenton reaction for the degradation of dye molecules and the reduction of Cr(VI), Chin. Chem. Lett. 30 (12) (2019) 2205–2210, https://doi.org/10.1016/j.cclet.2019.09.052.

[47] M. Jia, Q. Liu, W. Xiong, Z. Yang, C. Zhang, D. Wang, Y. Xiang, H. Peng, J. Tong, J. Cao, H. Xu, Ti^{3+} self-doped TiO_2 nanotubes photoelectrode decorated with Ar-Fe_2O_3 derived from MIL-100(Fe): Enhanced photo-electrocatalytic performance for antibiotic degradation, Appl Catal B-Environ 310 (2022), 121344, https://doi.org/10.1016/j.apcatb.2022.121344.